

Article

Surface Characterization and Photoluminescence Properties of Ce³⁺,Eu Co-Doped SrF₂ Nanophosphor

Mubarak Y. A. Yagoub ^{1,2}, Hendrik C. Swart ^{1,*}, Luyanda L. Noto ¹, Peber Bergman ³
and Elizabeth Coetsee ^{1,*}

¹ Department of Physics, University of the Free State, PO Box 339, Bloemfontein, ZA 9300, South Africa; E-Mails: yagoubm@ufs.ac.za (M.Y.); luyanda.noto@gmail.com (L.N.)

² Department of Physics, Sudan University of Science and Technology, Khartoum 11113, Sudan

³ Department of Physics, Chemistry and Biology, Linköping University, Linköping S-581 83, Sweden; E-Mail: peber@ifm.liu.se

* Authors to whom correspondence should be addressed; E-Mails: swarthc@ufs.ac.za (H.C.S.); coetsee@ufs.ac.za (E.C.); Tel.: +27-51-4012926 (H.C.S.); Fax: +27-51-40123507 (H.C.S.).

Academic Editor: Dirk Poelman

Received: 28 January 2015 / Accepted: 10 April 2015 / Published: 30 April 2015

Abstract: SrF₂:Eu,Ce³⁺ nanophosphors were successfully synthesized by the hydrothermal method during down-shifting investigations for solar cell applications. The phosphors were characterized by X-ray diffraction (XRD), scanning Auger nanoprobe, time of flight-secondary ion mass spectrometry (TOF-SIMS), X-ray photoelectron spectroscopy (XPS) and photoluminescence (PL) spectroscopy. XRD showed that the crystallite size calculated with Scherrer's equation was in the nanometre scale. XPS confirmed the formation of the matrix and the presence of the dopants in the SrF₂ host. The PL of the nanophosphor samples were studied using different excitation sources. The phenomenon of energy transfer from Ce³⁺ to Eu²⁺ has been demonstrated.

Keywords: SrF₂; cerium; TOF-SIMS; XPS; shake-down; energy transfer

1. Introduction

Strontium fluoride (SrF₂) is one of the most widely used optical materials because of its interesting luminescent, optical, and physical properties. It has a wide band gap, low phonon energy, low

refraction index, high radiation resistance, and good mechanical strength [1,2]. The photoluminescence properties of SrF₂ doped by Ln³⁺ ions have been extensively investigated in which charge compensation is required when Ln³⁺ ions substitute Sr²⁺ cation. This gives rise to a rich multisite structure. It has therefore been considered as a good phosphor host material that can be doped by a number of lanthanide ions for various luminescent applications [1–4]. SrF₂ host material doped with Ce³⁺ lanthanide ions is an example of a phosphor material that is extensively being investigated specifically for light amplification [5,6]. Some of these light amplification studies proposed that the SrF₂:Ce³⁺ phosphor material could be a promising scintillator [5]. Shendrik *et al.* [5] reported efficient scintillation light output of SrF₂:Ce³⁺ with high temperature stability suggesting that this material can be applied in well-logging scintillation detectors. They have also reported that the optimal Ce³⁺ doping level for maximum luminescence was 0.3 mol% if prepared by the Stockbarger method. Ce³⁺ ions in SrF₂ showed a fully allowed broad band 4f–5d transition [5] and this transition strongly absorbs UV radiation that results in a high absorption coefficient.

In the other hand, several previous studies have described the luminescence of Eu³⁺ doped materials as a good downshifting ion [7–10]. Gao *et al.* [7] reported luminescence due to transitions from the ⁵D₀ excited level to the ⁷F_J levels, where spectral conversion of 325–550 nm light to 570–710 nm light has been demonstrated. In our previous investigation of SrF₂:Eu we reported the emissions from both the Eu oxidation states (Eu³⁺ and Eu²⁺) where emission from 400 to 710 nm was observed [10]. X-ray photoelectron spectroscopy (XPS) results confirmed that the samples contained both Eu²⁺ and Eu³⁺ ions. The Eu³⁺ ion doped materials emits narrow emission peaks in the range of the orange-red emission with large Stokes shifts (>150 nm) that originates from the 4f–4f weak absorption transitions [11,12], whereas the 4f–5d absorption transition of the Eu³⁺ ion in SrF₂ is situated at the far ultraviolet region, which can be less accessible. In some applications, high or suitable absorption cross-section is needed and this requires a sensitizer with a high absorption coefficient [2,9,13]. Therefore, the presence of the Eu²⁺ and Eu³⁺ ions in the SrF₂ host greatly enhanced the emission intensity of Eu³⁺ at high concentrations [10]. In this work, Ce³⁺ singly and co-doped Eu in SrF₂ was prepared by using the hydrothermal method. The surface and photoluminescence properties are discussed.

2. Results and Discussion

2.1. Structure Analysis

2.1.1. X-Ray Diffraction (XRD)

Figure 1 shows the XRD patterns of un-doped and doped SrF₂ as well as the standard data for SrF₂ from card 00-086-2418. Doping with Ce- or Eu ions as well as the co-doped systems result in a small shift to higher angles with comparison to the un-doped sample and the standard data. This can be attributed to the radius difference between Eu (Eu²⁺ is 0.125 nm, Eu³⁺ is 0.107 nm), Ce³⁺ (0.114 nm) and Sr²⁺ (0.126 nm) ions, which confirms that Eu- and Ce ions are successfully incorporated into the SrF₂ lattice. It should be mentioned that doping with Eu- and Ce ions (up to 10 mol%) does not change the structure of the SrF₂ host in this study. The calculated SrF₂ lattice parameter is found to be (5.785 ± 0.005) Å and this agreed well with the reported value of (5.7996 ± 0.0001) Å [14].

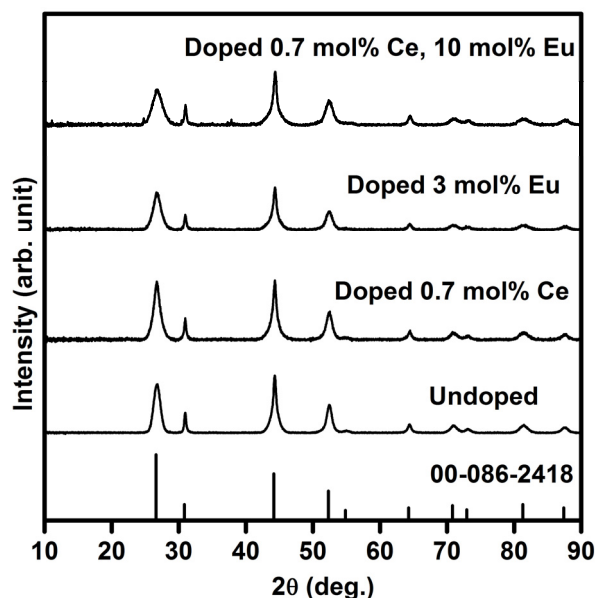


Figure 1. XRD patterns of pure and doped SrF₂.

The estimated average crystallite size (S) for pure and doped SrF₂ is calculated by using the diffraction peaks and Scherrer's equation [15], $S = 0.9\lambda/\beta\cos\theta$. S is the average crystallite size of the SrF₂ particles, λ is the wavelength of the X-rays (0.154 nm) and β is the full-width at half maximum of the X-ray peak at the Bragg angle θ . The average crystallite size of the pure SrF₂ was found to be 7.6 nm. The XRD peaks broaden with increasing the dopants ions (see Figure 1). The broadening of the XRD peaks were also observed by other groups [16,17]. H.A.A. Seed Ahmed *et al.* [16] attributed the XRD peak broadening to impurity broadening. Whereas, F. Wang *et al.* [17] assigned the XRD peak broadening to reduction in the nanoparticle size of the matrix. In our previous investigation of Eu doped SrF₂ samples, we assigned the XRD broadening as a result of a decrease in particle size of the matrix, which agreed well with F. Wang *et al.* [10]. Therefore, in the current study we can also assign these peaks' broadening to reduction in particle size of the matrix. The particle size reduced up to 3.9 nm for the SrF₂ sample that was doped with 0.7 mol% Ce³⁺ and 10 mol% Eu.

2.1.2. Auger and TOF SIMS analysis

An Auger profile of Ce and Eu co-doped SrF₂ was done to identify the sample's composition. The Auger spectrum of the SrF₂:Ce³⁺,Eu is presented in Figure 2. The Auger peaks at 71, 1515, 1644 and 1713 eV are assigned to Sr while the F peak is situated at 656 eV [18]. The Auger spectrum not only confirmed the formation of the host matrix, but also showed the presence of the dopants. The Eu peaks were at 111, 142, 853 and 985 eV, while the peak at 89 eV corresponds to Ce. In addition C and O were also observed. The C contamination is attributed to adventitious hydrocarbons and the O is considered to be a common impurity in a fluoride compound [19,20]. The presence of the O in the sample did not change the structure of the sample (see Figure 1). Therefore, the O contamination was due to adventitious impurity species in the surface rather than oxygen impurity in the SrF₂ matrix.

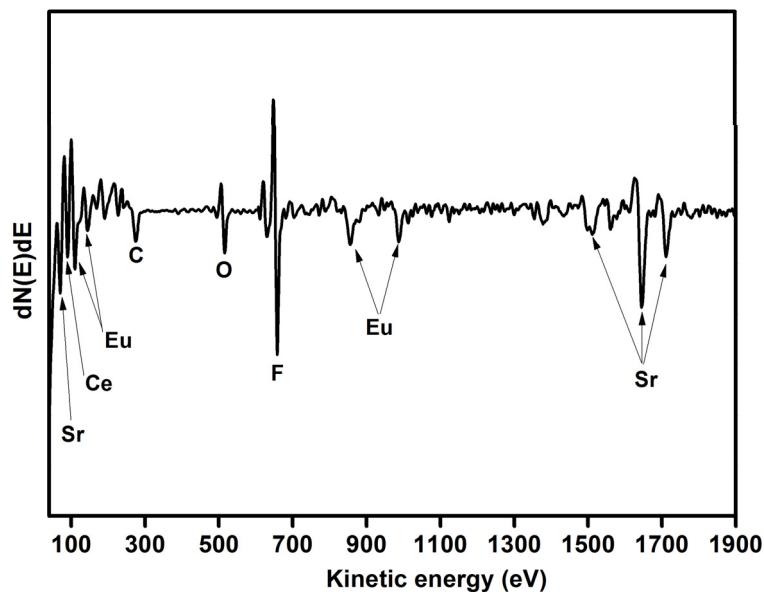


Figure 2. Auger spectrum of Ce and Eu co-doped SrF₂.

It could clearly be seen, not shown, that both the Ce and Eu ions were distributed quite homogeneously over the entire surface area of the Ce and Eu co-doped SrF₂. That indicated that the dopants were uniformly distributed in the SrF₂ matrix during the hydrothermal synthesis method.

2.1.3. X-ray Photoelectron Spectroscopy (XPS)

XPS measurements have been done in order to investigate the chemical composition and bonding state of the SrF₂:Ce,Eu phosphor powders. A higher dopant concentration (5 mol% for both Eu and Ce) was used in order to obtain a reasonable signal from the dopants. Figure 3 shows the peak fits for the (a) Sr 3*d*, (b) F 1*s*, (c) Eu 3*d* and (d) Ce 3*d* high resolution XPS peaks. The results also confirmed the presence of the host matrix elements (Sr and F) as well as the dopants (Eu and Ce) to their corresponding binding energies. During the peaks fit procedure, the C 1*s* peak at 284.8 eV was taken as a reference for all charge shift corrections. This is done because the C 1*s* peak resulted from hydrocarbon contamination and its binding energy generally remains constant, irrespective to the chemical state of the sample. In addition to that, all the Gaussian percentages were assumed to have a combined Gaussian-Lorentzian shape. The high resolution XPS peak for the Sr 3*d* showed two individual peaks. These two peaks are assigned to Sr 3*d* in SrF₂ that originate from the spin-orbit splitting 3*d*_{5/2} (133.5 eV) and 3*d*_{3/2} (135.3 eV), while the F 1*s* peak is situated at 684.7 eV. The spin-orbit splitting of Sr 3*d* is about 1.78 eV, it is in a good agreement with reported value of 1.75 eV [21].

The peak deconvolution for the Eu 3*d* high resolution XPS peaks are shown in Figure 3c. The 3*d* level of Eu ion is composed of four peaks. These four peaks can be attributed to Eu³⁺ and Eu²⁺ spin-orbit splitting 3*d*_{5/2} and 3*d*_{3/2} core level, respectively [21–24]. The spin-orbit splitting for both oxidation states Eu³⁺ and Eu²⁺ is about 29.96 eV. The Eu 3*d* results showed good agreement with our previous XPS investigation of SrF₂:Eu phosphors powder where Eu composed of its two oxidation states (Eu²⁺ and Eu³⁺) [10].

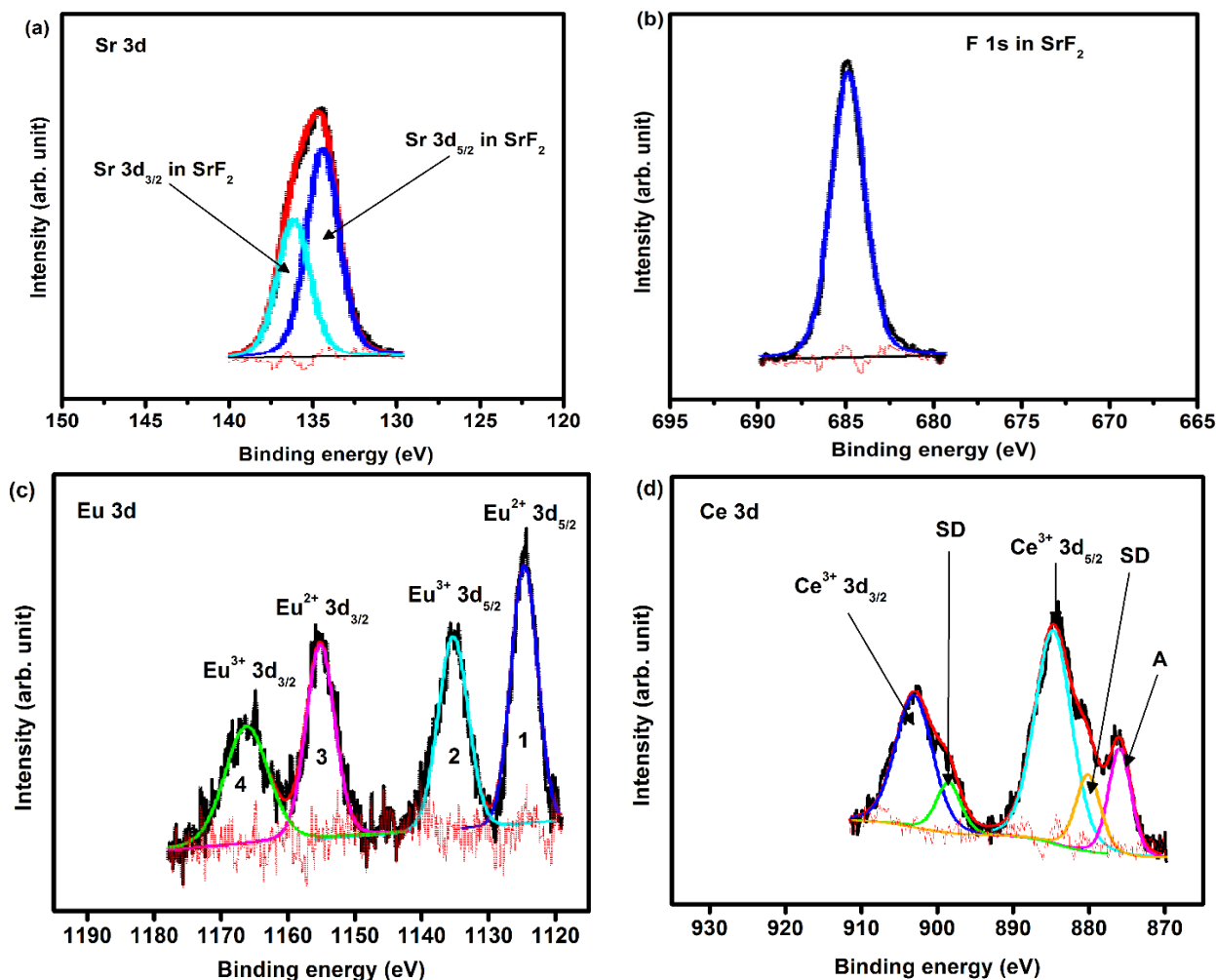


Figure 3. High resolution XPS peaks of (a) Sr 3d; (b) F 1s; (c) Eu 3d; and (d) Ce 3d for SrF₂:Ce,Eu phosphors powder.

The Ce 3d high resolution peak is shown in Figure 3d. The strong peaks correspond to the photoemission from the Ce³⁺ 3d state. Due to the spin-orbit interaction, the Ce³⁺ 3d photoemission peak consisted of two peaks that are assigned to the 3d_{3/2} and 3d_{5/2} peaks with 4f¹ final states, with an intensity ratio $I(3d_{5/2})/I(3d_{3/2}) = 3/2$ [22,25,26]. The spin-orbit splitting value (≈ 18.15 eV) is in good agreement with the estimated value (≈ 18.10 eV). The energy peaks labelled SD are due to the strong Coulomb interaction between photoemission in the 3d level and electrons located near the Fermi level. These peaks originate from the screening of the 3d level by valence band electrons to the 4f states [22]. This is possible due to hybridization of the Ce 4f level with the conduction band states [26]. In the photoemission nomenclature, these peaks are a result from what is called, shake-down process [22]. The 3d shake-down peaks behave the same as the 3d spin-orbit splitting peaks but they are a result from the 3d⁹f² final state. Therefore, the SD peaks can be assigned to the 3d_{3/2} and 3d_{5/2} XPS peaks with 4f² final states and this is in accordance with previous work done in Ce [25,26]. The shoulder peaks marked as A is related to the F KLL Auger electron peak. The XPS peak positions, area distributions and chemical bonding for all the peaks in as-prepared SrF₂:Ce,Eu are tabulated in Table 1.

Table 1. XPS peak position, area distribution and chemical bonding of as-prepared SrF₂:Ce,Eu phosphor powder.

Element	B.E (±0.1 eV)	Area distribution	Interpretation
F1s	684.7	2688	F in SrF ₂
Sr3d	133.5	1986	Sr 3d _{5/2} in SrF ₂
	135.3	1311	Sr 3d _{3/2} in SrF ₂
Eu3d	1123.3	1613	Eu ²⁺ 3d _{5/2} in fluoride
	1133.05	1372	Eu ³⁺ 3d _{5/2} in fluoride
	1153.2	1064	Eu ²⁺ 3d _{3/2} in fluoride
Ce3d	1163.0	905	Eu ³⁺ 3d _{3/2} in fluoride
	880.3	1296	Shake-down satellite
	884.8	5141	Ce ³⁺ 3d _{5/2} in fluoride
	898.5	855	Shake-down satellite
	903.0	3393	Ce ³⁺ 3d _{3/2} in fluoride
	876.1	1592	F KL ₁ L ₁ Auger electron peak

2.2. Photoluminescence Spectroscopy

2.2.1. SrF₂:Ce³⁺

The emission and excitation spectra of the Ce³⁺ singly doped SrF₂ nanophosphor are shown in Figure 4. The excitation spectrum consists of a prominent peak that is centred at 295 nm. This peak has been previously assigned to Ce³⁺:4f–5d excitation transition in SrF₂ [27]. By exciting the samples by 295 nm, a broad band emission peak is observed, which is attributed to the inter-configuration 5d¹–4f¹ allowed transition of Ce³⁺ ions. The inset graph in Figure 4 shows the emission intensity variation as a function of the Ce³⁺ concentration. The maximum luminescence intensity occurred for the sample doped with 0.7 mol% and a further increase in concentration resulted in a decrease in Ce³⁺ emission intensity. A previous study done by R. Shendrik *et al.* [5] on the SrF₂:Ce³⁺ sample reported that Ce³⁺ has a broad emission band that consist of two emission peaks (Ce³⁺ 5d to 4f ground state (²F_{7/2} and ²F_{5/2})) and the maximum intensity was observed at a Ce³⁺ dopant concentration of 0.3 mol%. In this study, the peaks were broadened and they fully overlapped, which might be the reason that only one broad peak was observed.

2.2.2. SrF₂:Ce,Eu

Figure 5a shows the PL emission spectra of SrF₂:Eu obtained by using the He-Cd laser PL system with a 325 nm excitation wavelength. The spectra clearly consist of a broad emission band that is centred at 416 nm with narrow bands in the range of 550–710 nm. The broad emission band is assigned to the inter-configuration 4f⁶5d¹–4f⁷ allowed transition of Eu²⁺ [11,12] and the narrow emission bands to the Eu³⁺ emission originating from the 4f–4f transition [28]. The Eu³⁺ emission consists of orange–red emission bands that is attributed to the ⁵D₀→⁷F_J transitions (J = 1, 2, 3, 4). This implies that the SrF₂:Eu samples consist of both Eu oxidation states (Eu²⁺ and Eu³⁺), with their emission ranging from 400 to 710 nm [10]. The Eu³⁺ emission bands increased with an increase in the Eu dopant concentration in the SrF₂ matrix. This can also be seen in Figure 5b, where the emission of Eu³⁺

excited by 394 nm is portrayed. The PL emission intensity increased slightly at the lower concentrations but then increased dramatically at 10 mol%. The presence of both Eu oxidation states therefore strongly enhanced the emission intensity of the Eu^{3+} ions. Detailed investigations on the luminescence phenomenon of Eu^{3+} and Eu^{2+} have previously been studied by various workers [10,29–31].

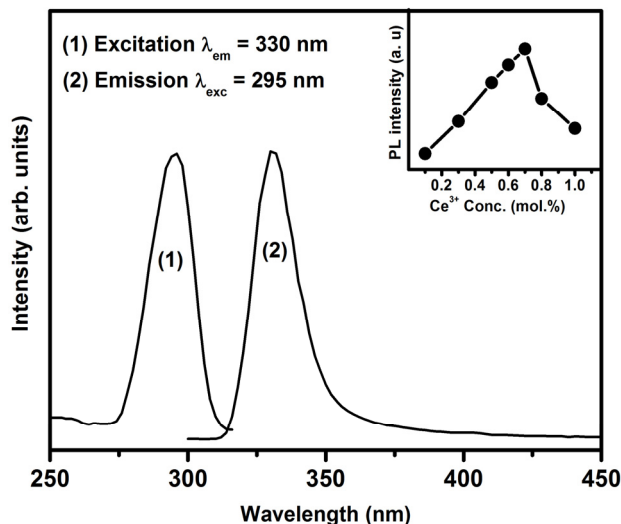


Figure 4. Excitation and emission spectra of the $\text{SrF}_2:\text{Ce}^{3+}$ (0.7 mol%) nanophosphor. The inset shows the 5d–4f transition's emission intensity as a function of Ce^{3+} concentration.

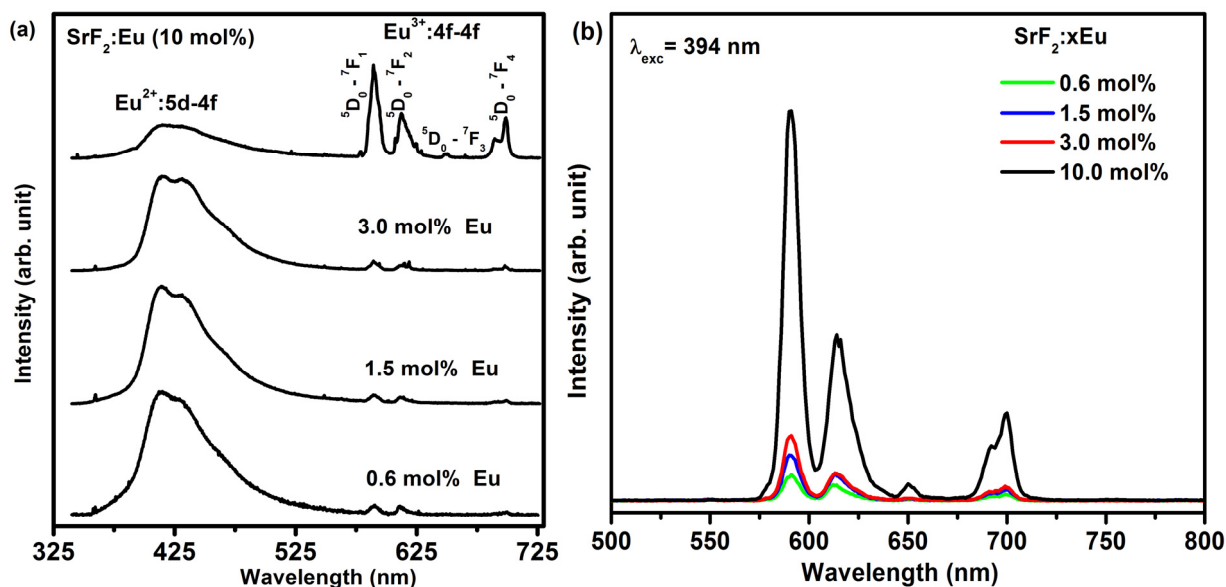


Figure 5. Photoluminescence spectra of $\text{SrF}_2:\text{xEu}$ excited by (a) using the He-Cd laser system with 325 nm excitation wavelength and (b) the Cary Eclipse with a wavelength of 394 nm.

Figure 6a depicts the PL emission of Ce^{3+} (0.7%) co-doped $\text{SrF}_2:\text{xEu}$ (where $x = 0.2\%$, 0.6%, 5% and 10%) excited with the He-Cd laser system with a 325 nm wavelength. The spectra also consisted of both the Eu^{2+} and Eu^{3+} emissions. A shoulder peak (marked with a dollar sign (\$)) at a lower wavelength only appeared for the smaller dopant concentrations' (0.2 and 0.6 mol%). This shoulder (\$) is assigned to the 4f–5d emission of Ce^{3+} , which is completely quenched at the higher Eu

concentration. With an increasing concentration of the Eu ions the relative PL emission intensity of the Eu^{2+} gradually decreased and the Eu^{3+} emission intensity increased. The emission intensity of the Eu^{3+} has dramatically increased at the high Eu doping concentration. This can clearly be seen in Figure 6b where the Eu^{3+} emission intensity plotted as function of Eu concentration for the Eu co-doped Ce^{3+} system. It can be noticed that Ce^{3+} co-doped $\text{SrF}_2:\text{Eu}$ greatly enhanced the Eu^{3+} ions emission intensity at high Eu concentration. The increase of the Eu^{3+} emission intensity with an increase in the Eu concentration can be attributed to an increase in the $\text{Eu}^{3+}/\text{Eu}^{2+}$ ratio in the presence of the Ce^{3+} ions. In the SrF_2 crystal, the Sr^{2+} ion is located at the body centre of a cube of eight F^- ions. The trivalent Ln^{3+} ions normally replace the Sr^{2+} cation. The extra charge of the Ln^{3+} ions is compensated by F^- anion charges situated elsewhere in an interstitial site. With increasing Ln^{3+} concentration, some kind of structural deformation occurs, the $\text{Ln}^{3+}-\text{F}$ dipoles couple to dimers, trimers and higher aggregates. The interstitial F^- ions and vacancies on the normal F^- site compose cuboctahedral clusters [32]. However, at low Eu concentration (less than Ce^{3+} concentration), the clusters are not completely formed. Besides, compare with the size of the Eu^{3+} (0.107 nm), the size of the Eu^{2+} (0.125 nm) is much closer to the size of the Sr^{2+} (0.126 nm), and hence the reduction of Eu^{3+} to Eu^{2+} ions is favored because it could reduce the lattice distortion of the doped SrF_2 crystal [33]. At high Eu concentration (bigger than the Ce^{3+} concentration), the dimensions of the Eu^{3+} ions cluster increased and hence the ratio of $\text{Eu}^{3+}/\text{Eu}^{2+}$ increased. The increase of the Eu^{3+} ions therefore increased the Eu^{3+} emission intensity.

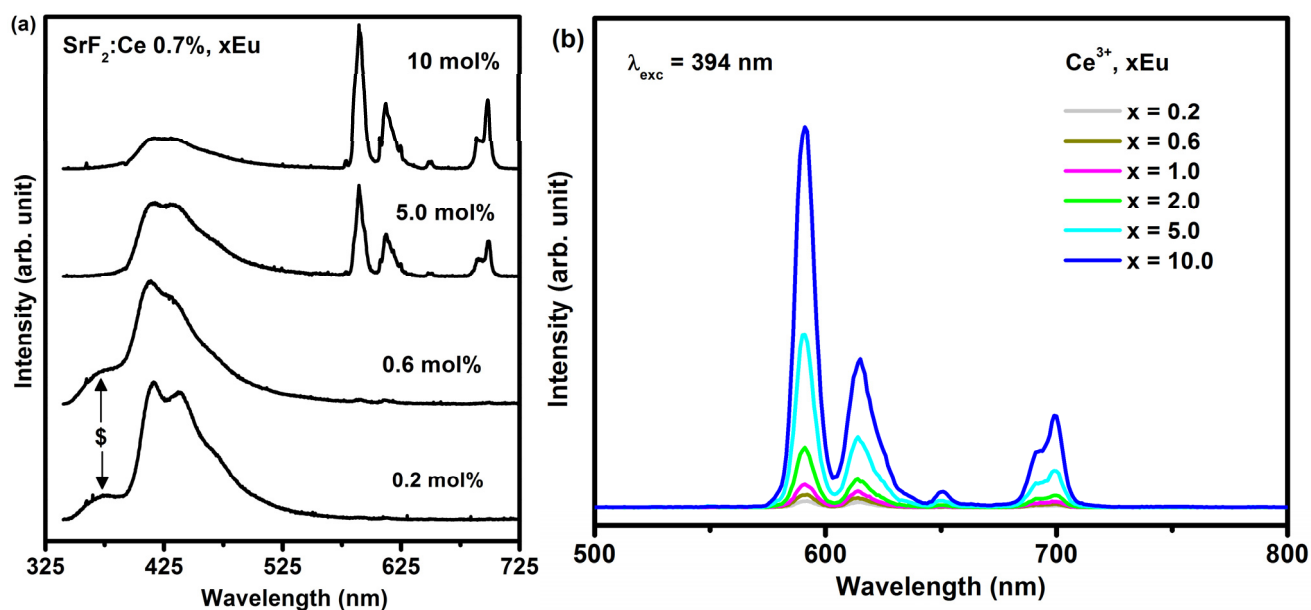


Figure 6. (a) PL spectra of $\text{SrF}_2:\text{Ce}^{3+}$ (0.7 mol%), $x\text{Eu}$ excited with the laser system with a 325 nm excitation wavelength and (b) 394 nm using the xenon lamp.

The PL emission spectra of the $\text{SrF}_2:\text{Ce}^{3+},\text{Eu}$ nanophosphor excited by the 295 nm excitation wavelength are plotted in Figure 7a. The broad emission band that is centered at a wavelength of 330 nm is a characteristic of the Ce^{3+} ion which is in agreement with the emission spectra for Ce^{3+} in Figure 4. The additional broad peak beside the Ce^{3+} emission that was centered at 416 nm is assigned to the Eu^{2+} ions in SrF_2 (clearly shown in the inset graph of Figure 7a). The Eu^{2+} emission slightly increased before it decreased with increasing Eu concentration. In Figure 7a the emission spectrum of

the SrF₂:Eu without Ce excited at 295 nm is also shown. It clearly shows no Eu²⁺ emission has occurred. The presence of Eu²⁺ emission under 295 nm excitation, in the co-doped samples, is therefore evidence of an energy transfer process from Ce³⁺ to Eu²⁺. This process can occur in such material since the emission of Ce³⁺ overlaps the excitation spectra of Eu²⁺ (Figure 7b; SrF₂:Ce³⁺ (0.7 mol%), Eu (0.6 mol%)). Such spectral overlap is a necessary condition for the occurrence of the energy transfer from Ce³⁺ to Eu²⁺. An efficient energy transfer from Ce³⁺ to Eu²⁺ in a fluoride crystal was previously demonstrated even for a very low concentration [34]. More evidence of energy transfer between Ce³⁺ and Eu²⁺ is shown in Figure 7c where the room temperature luminescence excitation spectra of SrF₂:Ce³⁺ (0.7 mol%), Eu (0.6 mol%) nanophosphors are plotted. The excitation spectrum of Eu²⁺ (dotted line) not only consists of the Eu²⁺:4f⁷→4f⁶5d excitation transition but also the Ce³⁺ excitation band (clearly seen in the inset of the Figure 7c). All these results confirm the existence of energy transfer from Ce³⁺ to the Eu²⁺ ion.

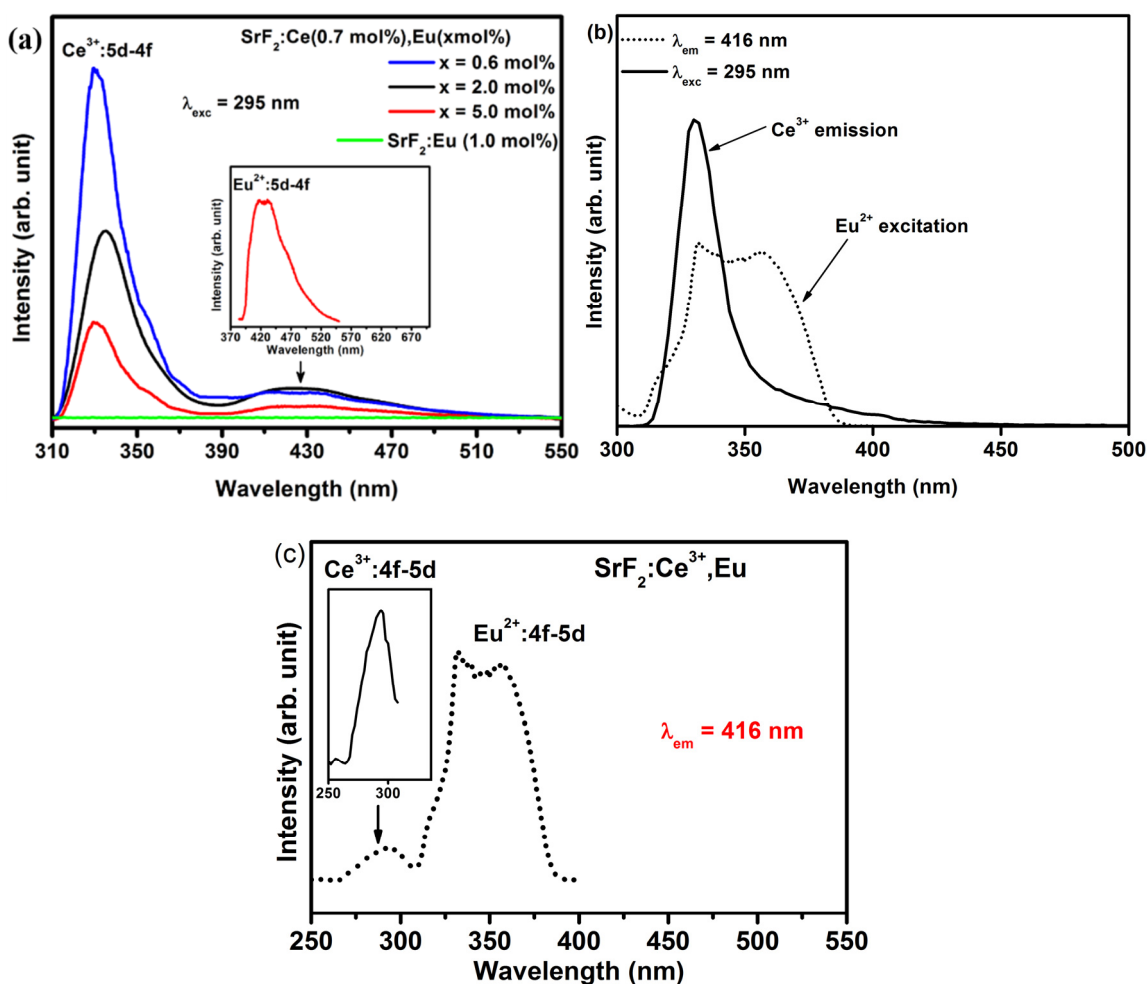


Figure 7. (a) PL emission spectra of Ce³⁺ and Eu²⁺ from SrF₂:Ce³⁺ (0.7 mol%) with different Eu doping concentration as well as from Eu²⁺ in SrF₂:Eu excited by an excitation wavelength of 295 nm; (b) Spectral overlap between Ce³⁺ emission and Eu²⁺ excitation and (c) excitation spectra of SrF₂:Ce³⁺ (0.7 mol%), Eu (0.6 mol%) nanophosphors measured at an emission wavelength of 416 nm. The inset in (a) is the enlarge spectrum of the Eu²⁺ emission ions and the inset in (c) is the enlarge Ce³⁺ excitation from SrF₂:Ce³⁺ (0.7 mol%), Eu (5.0 mol%).

Results obtained from the luminescence decay curves for Ce^{3+} emission also contributed further to the energy transfer process. The decay time of the donor ions does not change in the presence and absence of the acceptor ions if the radiative energy is dominant [35]. In the situation of non-radiative energy transfer the decay time of the donor ions gradually decreases with an increase in the acceptor concentration. The PL decay curves of Ce^{3+} with various Eu concentration are shown in Figure 8. The decay curve of the Ce^{3+} ions gradually decreased with an increase in the Eu concentration. The luminescence decay curve of Ce^{3+} singly doped SrF_2 nanoparticles can well be fitted into a single-exponential function, shown in the inset of Figure 8, whereas the decay curve of the entire co-doped concentrations were fitted with a bi-exponential decay model [35,36]:

$$I(t) = A_1 \exp(-t/\tau_1) + A_2 \exp(-t/\tau_2) \quad (1)$$

$I(t)$ is the luminescence intensity at time t ; A_1 and A_2 are constants; and τ_1 and τ_2 are the short- and long-decay components, respectively. The average lifetime constant ($\bar{\tau}$) can be calculated from the following equation:

$$\bar{\tau} = (A_1 \tau_1^2 + A_2 \tau_2^2)/(A_1 \tau_1 + A_2 \tau_2) \quad (2)$$

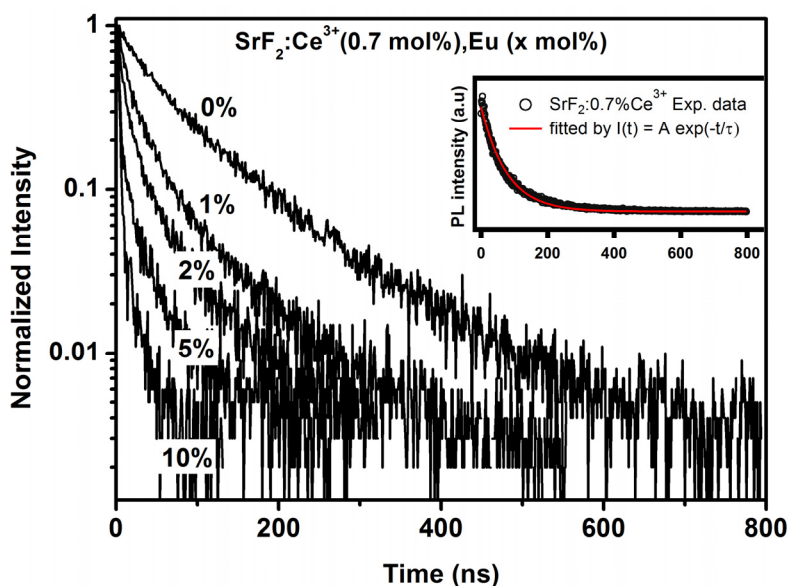


Figure 8. The decay lifetime of Ce^{3+} ions in the SrF_2 host with an increase in Eu concentration. The inset graph shows the decay curve of 0.7% Ce^{3+} in SrF_2 fitted to a single-exponential fitting function.

The lifetime of the Ce^{3+} doped SrF_2 is determined to be 77.15 ns. This value is in good agreement with the reported value of Ce^{3+} in SrF_2 [27]. In the Eu ions co-doped system, the average lifetime of the donor ion (Ce^{3+}) decreased up to 8.2 ns at 10 mol% Eu concentration. This results confirm that the excitation energy of Ce^{3+} ions was transferred to the Eu^{2+} ions. The lifetime results for the Ce^{3+} ions in the SrF_2 host strongly suggest that the energy transfer from Ce^{3+} to Eu^{2+} was non-radiative. The energy transfer efficiency from Ce^{3+} to Eu is defined by the following expression:

$$\eta_{\text{ET}} = 1 - \tau/\tau_0 \quad (3)$$

where τ and τ_0 are the average lifetime of Ce^{3+} in the presence and absence of the Eu ions, respectively. The corresponding lifetime and energy transfer efficiencies are tabulated in Table 2. From Table 2, the energy transfer of Ce^{3+} increased gradually with an increase in the Eu concentration. The maximum energy transfer efficiency is about 89.4% for the sample doped with 0.7 mol% Ce^{3+} and 10 mol% Eu. An efficient energy transfer has occurred from Ce^{3+} to Eu^{2+} . The emission of Eu^{2+} has slightly increased before it decreased with increasing Eu concentration due to the decrease of the Eu^{2+} ratio in the SrF_2 host. In our previous investigation of $\text{SrF}_2:\text{Eu}$ the Eu^{2+} ion was, however, found to be unstable when irradiated by a YAG laser. The Eu^{2+} ion's PL emission intensity rapidly decreased with time and this result made the $\text{SrF}_2:\text{Eu}$ nanophosphor an unsuitable candidate for several applications, such as white light-emitting diodes and wavelength conversion films for silicon photovoltaic cells [10].

Table 2. Lifetime of the 5d–4f transition of Ce^{3+} (330 nm) and the Ce^{3+} -Eu energy transfer efficiency (η_{ET}) in SrF_2 matrix.

Eu concentration (mol%)	τ (ns)	η_{ET} (%)
0	77.15	0
1	46.3	40
2	31.9	58.6
5	16.05	79.2
10	8.2	89.4

3. Experimental Section

Doped and un-doped SrF_2 phosphor samples were synthesised by the hydrothermal method. For the hydrothermal process, all chemical reagents were of analytical grade and were used without further purification. For a typical synthesis, 1 mmol of $\text{Sr}(\text{NO}_3)_2$ was first dissolved in 30 mL distilled water, followed by 5 mmol of $\text{C}_{10}\text{H}_{14}\text{N}_2\text{O}_8 \cdot 2\text{H}_2\text{O}$ (Na_2EDTA , ethylenediamine tetraacetic acid disodium salt) and 2 mmol of NaBF_4 under constant stirring. After further magnetic stirring for 10 min the solution was transferred into a 125 mL autoclave lined with Teflon, heated at 160 °C for one hour and naturally cooled down to room temperature [37]. The product was collected by centrifugal and washed with water and ethanol. Finally, the product was dried for 10 h in an oven at 60 °C. Ce^{3+} and Eu co-doped SrF_2 samples were prepared by the same hydrothermal technique. $\text{Eu}(\text{NO}_3)_3(\text{H}_2\text{O})_5$ and $\text{Ce}(\text{NO}_3)_3(\text{H}_2\text{O})_6$ were used as sources for the Eu and Ce dopants, respectively.

The phosphors were characterized by X-ray diffraction (XRD) (Bruker AXS GmbH, Karlsruhe, Germany) (Bruker Advance D8 diffractometer with Cu K_α radiation ($\lambda = 0.154$ nm)) to identify the crystalline structure of the powder. Auger spectra were collected with a PHI 700 Scanning Auger Nanoprobe (ULVAC-PHI Inc, Chanhassan, MN, USA) equipped with a scanning Auger microscope (SAM). The field emission electron gun used for the SAM analyses was set at: 2.34 A filament current; 4.35 kV extractor voltage and 381.4 μA extractor current. With these settings a 25 kV, 10 nA electron beam was obtained for the Auger analyses. The electron beam diameter was about 10 nm. An IonTof time of flight secondary ion mass spectrometer (TOF-SIMS) instrument (ION-TOF GmbH, Muenster, Germany) equipped with a Bi primary ion source was used to characterize the nanophosphor materials for their chemical composition and dopants distribution. In spectroscopy mode, the system equipped with a DC current of 30 nA and a pulsed current of 1 pA at 30 kV with a heating current of 2.95 A and

emission current of 0.8 μA was used. High resolution X-ray photoelectron spectroscopy (XPS) was obtained with a PHI 5000 Versaprobe system (ULVAC-PHI Inc, Chanhassan, MN, USA). A low energy Ar^+ ion gun and low energy neutralizer electron gun were used to minimize charging on the surface. A 100 μm diameter monochromatic Al $K\alpha$ X-ray beam ($h\nu = 1486.6$ eV) generated by a 25 W, 15 kV electron beam was used to analyze the different binding energy peaks. The pass energy was set to 11 eV giving an analyzer resolution ≤ 0.5 eV. Multipack version 8.2 software (ULVAC-PHI Inc, Chanhassan, MN, USA) was utilized to analyze the spectra to identify the chemical compounds and their electronic states using Gaussian-Lorentz fits. Photoluminescence spectra (PL) were collected using a Cary Eclipse fluorescence spectrophotometer (Varian Ltd, Mulgrave Victoria, Australia) equipped with a xenon lamp and also with a He-Cd laser PL system with a 325 nm excitation wavelength. Luminescence decay curves were recorded by using a NanoLED with a 335 nm excitation wavelength and repetition rate of 1 MHz. All measurements were performed at room temperature.

4. Conclusions

As-prepared $\text{SrF}_2:\text{Eu,Ce}$ nanophosphors were successfully synthesised with the hydrothermal technique. The average crystallite size that was calculated by using Scherrer's equation was found to be 7.6 nm for the host sample. Dopant ions were intended to decrease the particle size of the host. The Auger spectra confirmed the presence of Sr, F, Eu and Ce elements in the host matrix. Photoluminescence properties of Ce^{3+} and Eu co-doped SrF_2 nano-phosphor have been investigated. A possible efficient energy transfer from Ce^{3+} to Eu^{2+} ions was demonstrated. From the PL decay curves the energy transfer efficiency was calculated to be 89.4% for the SrF_2 : 0.7 mol% Ce^{3+} , 10 mol% Eu sample.

Acknowledgments

This work is based on the research supported by the South African Research Chairs Initiative of the Department of Science and Technology and National Research Foundation of South Africa. The financial assistance of the National Research Foundation (NRF) and the University of the Free State towards this research is hereby acknowledged.

Author Contributions

Hendrik C. Swart is the leader of the research group and supervisor of the PhD students and he helped with the data interpretation and writing of the paper. Elizabeth Coetsee is also one of the supervisors of the PhD students and she helped with the editing of the paper. Luyanda Noto helped with the TOF-SIMS analysis and discussion and Mubarak Y. A. Yagoub was mainly responsible for the planning, experimental part as well as writing the main part of the paper, the decay measurements were done with the help of Peber Bergman in his laboratory.

Conflicts of Interest

The authors declare no conflict of interest.

References

1. Ivanovskikh, K.V.; Pustovarov, V.A.; Krim, M.; Shulgin, B.V. Time-resolved vacuum ultraviolet spectroscopy of Er³⁺ ions in the SrF₂ crystal. *J. Appl. Spectrosc.* **2005**, *72*, 564–568.
2. Van der Ende, B.M.; Aarts, L.; Meijerink, A. Near-infrared quantum cutting for photovoltaics. *Adv. Mater.* **2009**, *21*, 3073–3077.
3. Ivanovskikh, K.; Pustovarov, V.; Smirnov, A.; Shulgin, B. Inter- and intraconfigurational luminescence of trivalent rare earth ions doped into strontium fluoride crystals under vacuum ultraviolet excitation. *Phys. Stat. Solidi C* **2007**, *4*, 889–892.
4. Kristianpoller, N.; Weiss, D.; Chen, R. Optical and dosimetric properties of variously doped SrF₂ crystals. *Radiat. Meas.* **2004**, *38*, 719–722.
5. Shendrik, R.; Radzhabov, E.A.; Nepomnyashchikh, A.I. Scintillation properties of pure and Ce³⁺-doped SrF₂ crystals. *Radiat. Meas.* **2013**, *56*, 58–61.
6. Shendrik, R.; Radzhabov, E. Emission in CaF₂, BaF₂, SrF₂. *IEEE Trans. Nucl. Sci.* **2009**, *57*, 1295–1299.
7. Gao, D.; Zheng, H.; Zhang, X.; Fu, Z.; Zhang, Z.; Tian, Y.; Cui, M. Efficient fluorescence emission and photon conversion of LaOF:Eu³⁺ nanocrystals. *Appl. Phys. Lett.* **2011**, *98*, 011907–011909.
8. Chung, P.; Chung, H.; Holloway, P.H. Phosphor coatings to enhance Si photovoltaic cell performance. *J. Vac. Sci. Technol. A* **2007**, *25*, 61–66.
9. Huang, X.Y.; Wang, J.X.; Yu, D.C.; Ye, S.; Zhang, Q.Y.; Sun, X.W. Spectral conversion for solar cell efficiency enhancement using YVO₄:Bi³⁺,Ln³⁺ (Ln = Dy, Er, Ho, Eu, Sm, and Yb) phosphors. *J. Appl. Phys.* **2011**, *109*, 113526–113532.
10. Yagoub, M.Y.A.; Swart, H.C.; Noto, L.L.; O'Connell, J.H.; Lee, M.E.; Coetsee, E. The effects of Eu-concentrations on the luminescent properties of SrF₂:Eu nanophosphor. *J. Lumin.* **2014**, *156*, 150–156.
11. Li, Y.C.; Chang, Y.H.; Lin, Y.F.; Chang, Y.S.; Lin, Y.J. Synthesis and luminescent properties of Ln³⁺ (Eu³⁺, Sm³⁺, Dy³⁺)-doped lanthanum aluminum germanate LaAlGe₂O₇ phosphors. *J. Alloys Compd.* **2007**, *439*, 367–375.
12. Jin, Y.; Qin, W.; Zhang, J. Preparation and optical properties of SrF₂:Eu³⁺ nanospheres. *J. Fluor. Chem.* **2008**, *129*, 515–518.
13. Huang, X.; Han, S.; Huang, W.; Liu, X. Enhancing solar cell efficiency: The search for luminescent materials as spectral converters. *Chem. Soc. Rev.* **2013**, *42*, 173–201.
14. Rakov, N.; Guimaraes, R.B.; Franceschini, D.F.; Maciel, G.S. Er:SrF₂ luminescent powders prepared by combustion synthesis. *Mater. Chem. Phys.* **2012**, *135*, 317–321.
15. Oprea, C.; Ciupina, V.; Prodan, G. Investigation of nanocrystals using TEM micrographs and electron diffraction technique. *Rom. J. Phys.* **2008**, *53*, 223–230.
16. Seed Ahmed, H.A.A.; Ntwaeaborwa, O.M.; Kroon, R.E. The energy transfer mechanism in Ce,Tb co-doped LaF₃ nanoparticles. *Curr. Appl. Phys.* **2013**, *13*, 1264–1268.
17. Wang, F.; Han, Y.; Lim, C.S.; Lu, Y.; Wang, J.; Xu, J.; Chen, H.; Zhang, C.; Hong, M.; Liu, X. Simultaneous phase and size control of upconversion nanocrystals through lanthanide doping. *Nature* **2010**, *463*, 1061–1065.

18. Childs, K.D.; Carlson, B.A.; LaVanier, L.A.; Moulder, J.F.; Paul, D.F.; Stickle, W.F.; Watson, D.G. *Handbook of Auger Electron Spectroscopy*, 3rd ed.; Physical Electronics: Eden Prairie, MN, USA, 1995.
19. Kroon, R.E.; Swart, H.C.; Ntwaeaborwa, O.M.; Seed Ahmed, H.A.A. Ce decay curves in Ce, Tb co-doped LaF₃ and the energy transfer mechanism. *Phys. B* **2014**, *439*, 83–87.
20. Van Wijngaarden, J.T.; Scheidelaar, S.; Vlugt, T.J.H.; Reid, M.F.; Meijerink, A. Energy transfer mechanism for downconversion in the (Pr³⁺, Yb³⁺) couple. *Phys. Rev. B* **2010**, *81*, 155112–155117.
21. Vasquez, R.P. SrF₂ by XPS. *Surf. Sci. Spectr.* **1992**, *1*, 24–30.
22. Vercaemst, R.; Poelman, D.; van Meirhaeghe, R.L.; Fiermans, L.; Laflere, W.H.; Cardon, F. An XPS study of the dopants' valence states and the composition of CaS_{1-x}Se_x:Eu and SrS_{1-x}Se_x:Ce thin film electroluminescent devices. *J. Lumin.* **1995**, *63*, 19–30.
23. Lu, D.; Sugano, M.; Sun, X.Y.; Su, W. X-ray photoelectron spectroscopy study on Ba_{1-x}Eu_xTiO₃. *Appl. Surf. Sci.* **2005**, *242*, 318–325.
24. Zhang, J.; Yang, M.; Jin, H.; Wang, X.; Zhao, X.; Liu, X.; Peng, L. Self-assembly of LaBO₃:Eu twin microspheres synthesized by a facile hydrothermal process and their tunable luminescence properties. *Mater. Res. Bull.* **2012**, *47*, 247–252.
25. Lässer, R.; Fuggle, J.C.; Beyss, M.; Campagna, M. X-ray photoemission from Ce core levels of CePd₃, CeSe, CeAl₂ and CeCu₂Si₂. *Phys. B C* **1980**, *102*, 360–366.
26. Gamza, M.; Slebarski, A.; Rosner, H. Electronic structure of Ce₃Rh₄Sn₁₀ from XPS and band structure calculations. *Eur. Phys. J. B* **2008**, *63*, 1–9.
27. Zhang, C.; Hou, Z.; Chai, R.; Cheng, Z.; Xu, Z.; Li, C.; Huang, L.; Lin, J. Mesoporous SrF₂ and SrF₂:Ln³⁺ (Ln = Ce, Tb, Yb, Er) Hierarchical microspheres: Hydrothermal synthesis, growing mechanism, and luminescent properties. *J. Phys. Chem. C* **2010**, *114*, 6928–6936.
28. Dorenbos, P. Energy of the first 4f⁷ → 4f⁶5d transition of Eu²⁺ in inorganic compounds. *J. Lumin.* **2003**, *104*, 239–260.
29. Dorenbos, P. Valence stability of lanthanide ions in inorganic compounds. *Chem. Mater.* **2005**, *17*, 6452–6456.
30. Baran, A.; Barzowska, J.; Grinberg, M.; Mahlik, S.; Szczodrowski, K.; Zorenko, Y. Binding energy of Eu²⁺ and Eu³⁺ ions in β-Ca₂SiO₄ doped with europium. *Opt. Mater.* **2013**, *35*, 2017–2114.
31. Biswas, K.; Sontakke, A.D.; Sen, R.; Annapurna, K. Luminescence properties of dual valence Eu doped nano-crystalline BaF₂ embedded glass-ceramics and observation of Eu²⁺→Eu³⁺ energy transfer. *J. Fluoresc.* **2012**, *22*, 745–752.
32. Pandey, C.; Dhopte, S.M.; Muthal, P.L.; Kondawar, V.K.; Moharil, S.V. Eu³⁺↔Eu²⁺ redox reactions in bulk and nano CaF₂:Eu. *Radiat. Eff. Defects Solids* **2007**, *162*, 651–658.
33. Wang, X.; Wu, N.; Shimizu, M.; Sakakura, M.; Shimotsuma, Y.; Miura, K.; Zhou, S.; Qiu, J.; Hirao, K. Space selective reduction of europium ions via SrF₂ crystals induced by high repetition rate femtosecond laser. *J. Ceram. Soc. Jpn.* **2011**, *119*, 939–941.
34. Caldino, U.G.; Gruz, C.D.; Monoz, G.H.; Rubio, J.O. Ce³⁺→Eu²⁺ energy transfer in CaF₂. *Solid State Commun.* **1989**, *4*, 347–351.
35. Zhou, J.; Xia, Z.; You, H.; Shen, K.; Yang, M.; Liao, L. Synthesis and tunable luminescence properties of Eu²⁺ and Tb³⁺-activated Na₂Ca₄(PO₄)₃F phosphors based on energy. *J. Lumin.* **2013**, *135*, 20–25.

36. Katsumata, T.; Nabaie, T.; Sasajima, K.; Komuro, S.; Morikawa, T. Effects of composition on the long phosphorescent $\text{SrAl}_2\text{O}_4:\text{Eu}^{2+}, \text{Dy}^{3+}$ Phosphor Crystals. *J. Electrochem. Soc.* **1997**, *144*, L243–L245.
37. Peng, J.; Hou, S.; Liu, X.; Feng, J.; Yu, X.; Xing, Y.; Su, Z. Hydrothermal synthesis and luminescence properties of hierarchical SrF_2 and $\text{SrF}_2:\text{Ln}^{3+}$ ($\text{Ln} = \text{Er}, \text{Nd}, \text{Yb}, \text{Eu}, \text{Tb}$) micro/nanocomposite architectures. *Mater. Res. Bull.* **2012**, *47*, 328–332.

© 2015 by the authors; licensee MDPI, Basel, Switzerland. This article is an open access article distributed under the terms and conditions of the Creative Commons Attribution license (<http://creativecommons.org/licenses/by/4.0/>).